



Estimating Subsurface Velocities from Surface Fields with Idealized Stratification

J. H. LACASCE

Department of Geosciences, University of Oslo, Oslo, Norway

J. WANG

Scripps Institute of Oceanography, University of California, San Diego, La Jolla, California

(Manuscript received 16 October 2014, in final form 20 June 2015)

ABSTRACT

A previously published method by Wang et al. for predicting subsurface velocities and density from sea surface buoyancy and surface height is extended by incorporating analytical solutions to make the vertical projection. One solution employs exponential stratification and the second has a weakly stratified surface layer, approximating a mixed layer. The results are evaluated using fields from a numerical simulation of the North Atlantic. The simple exponential solution yields realistic subsurface density and vorticity fields to nearly 1000 m in depth. Including a mixed layer improves the response in the mixed layer itself and at high latitudes where the mixed layer is deeper. It is in the mixed layer that the surface quasigeostrophic approximation is most applicable. Below that the first baroclinic mode dominates, and that mode is well approximated by the analytical solution with exponential stratification.

1. Introduction

Wang et al. (2013, hereinafter W13) proposed a method for projecting surface density and height downward in the water column. The method requires simultaneous observations of surface density (or temperature, in the absence of salinity) and height. The density projection is made using the surface quasigeostrophic (SQG) approximation (Blumen 1978; Held et al. 1995; Lapeyre and Klein 2006; LaCasce and Mahadevan 2006; Tulloch and Smith 2006; Isern-Fontanet et al. 2008). The height is then used to deduce the two gravest baroclinic modes. W13 found that the SQG portion was most important in the near-surface region, while the baroclinic modes dominated at depth.

Here we simplify the method by using analytic solutions for the vertical projection. This obviates determining the

SQG and baroclinic mode solutions numerically. We also consider a solution with a surface “mixed layer,” allowing us to gauge the latter’s effect on the construction.

2. Method

The method employs a two-component decomposition of the quasigeostrophic potential vorticity (Pedlosky 1987):

$$\nabla^2 \psi + \frac{\partial}{\partial z} \left(\frac{f_0^2}{N^2} \frac{\partial \psi}{\partial z} \right) = Q, \quad (1)$$

where $N(z)$ is the Brunt–Väisälä frequency, $\psi = p/(f_0 \rho_0)$ is the geostrophic streamfunction, and Q is the potential vorticity (PV). Because the PV equation is linear, the solution can be written as a superposition. The homogeneous solution is the SQG streamfunction ψ_s , while the particular solution is the “interior” streamfunction ψ_i (Lapeyre and Klein 2006). These have different surface boundary conditions:

$$\frac{\partial}{\partial z} \psi_i = 0, \quad \frac{\partial}{\partial z} \psi_s = \frac{b_s}{f_0}, \quad \text{at } z = 0, \quad (2)$$

Corresponding author address: Joe LaCasce, Department of Geosciences, University of Oslo, P.O. Box 1022 Blindern, N-0315 Oslo, Norway.
E-mail: j.h.lacase@geo.uio.no

where b_s is the surface buoyancy. Thus, only the SQG solution is directly linked to the surface density.

For the bottom boundary condition, W13 demanded that the vertical derivative of both streamfunctions vanish and that the total velocity be zero at the bottom. Alternately, one can simply require that each streamfunction vanish with depth (e.g., Lapeyre and Klein 2006; LaCasce and Mahadevan 2006; Lapeyre 2009):

$$\lim_{z \rightarrow -\infty} \hat{\psi}_i = \hat{\psi}_s = 0. \tag{3}$$

It turns out that using this condition greatly simplifies the subsequent solutions.

The interior solution cannot be determined because the interior PV Q is unknown, but the two gravest baroclinic modes can be deduced if the surface pressure is also known (W13). The baroclinic modes are solutions of the Sturm–Liouville problem:

$$\frac{\partial}{\partial z} \left(\frac{f_0^2}{N^2} \frac{\partial}{\partial z} F_n \right) + R_n^{-2} F_n = 0, \tag{4}$$

given

$$\psi_i(x, y, z, t) = \sum_n \gamma_n(x, y, t) F_n(z), \tag{5}$$

with the same boundary conditions as for ψ_i . Here R_n is the n th deformation radius and the γ_n are the modal coefficients.

With zero flow at depth, the baroclinic modes are surface intensified and the barotropic mode is absent (Pedlosky 1987; Samelson 1992; LaCasce 2012).¹ As such, there is only a single unknown, the amplitude of the first baroclinic mode γ_1 , which can be determined from the surface elevation η :

$$\begin{aligned} \psi_s(x, y, 0, t) + \psi_i(x, y, 0, t) &\approx \psi_s(x, y, 0, t) + \gamma_1 F_1(0) \\ &= \frac{g}{f_0} \eta(x, y, t). \end{aligned} \tag{6}$$

a. Exponential stratification

The SQG solution and baroclinic modes can be derived analytically for certain idealized stratifications. One is an exponential: $N = N_0 e^{z/h}$. Using this in (1) yields

$$\frac{d^2 \hat{\psi}}{dz^2} - \frac{2}{h} \frac{d\hat{\psi}}{dz} - \frac{N_0^2 \kappa^2}{f_0^2} e^{2z/h} \hat{\psi} = \frac{N_0^2 \kappa^2}{f_0^2} \hat{Q} e^{2z/h}. \tag{7}$$

Here $\psi = \sum_{k,l} \hat{\psi} \exp(ikx + ily)$ and $\kappa = (k^2 + l^2)^{1/2}$ is the total wavenumber. The PV and surface buoyancy are similarly transformed. The SQG solution $\hat{\psi}_s$ can be shown to be

$$\hat{\psi}_s = \frac{\hat{b}_s}{N_0 \kappa} e^{z/h} \frac{I_1(L_e \kappa e^{z/h})}{I_0(L_e \kappa)}, \tag{8}$$

where the I_n are modified Bessel functions and $L_e \equiv N_0 h / f_0$ is a deformation-like scale associated with the exponential stratification. The baroclinic modes, on the other hand, satisfy

$$\frac{d^2 F_n}{dz^2} - \frac{2}{h} \frac{dF_n}{dz} + \frac{N_0^2}{R_n^2 f_0^2} e^{2z/h} F_n = 0. \tag{9}$$

The solution that decays with depth has the form

$$F_n \propto e^{z/h} J_1 \left(\frac{L_e}{R_n} e^{z/h} \right), \tag{10}$$

where J_1 is a Bessel function of the first kind. Imposing the surface condition [(2)] yields

$$J_0 \left(\frac{L_e}{R_n} \right) = 0. \tag{11}$$

So, the R_n are determined from the zeros of J_0 . The first is 2.4048, so

$$R_1 = \frac{L_e}{2.4048}. \tag{12}$$

Notice that the eigenvalue problem is solved *without* a transcendental equation. This is because of the choice of lower boundary condition.

The full solution is then

$$\hat{\psi} = \frac{\hat{b}_s}{N_0 \kappa} e^{z/h} \frac{I_1(L_e \kappa e^{z/h})}{I_0(L_e \kappa)} + \gamma_1 e^{z/h} J_1(2.4048 e^{z/h}). \tag{13}$$

We determine γ_1 from (6):

$$\gamma_1 = \frac{1}{J_1(2.4048)} \left[\frac{g \hat{\eta}}{f_0} - \frac{\hat{b}_s}{N_0 \kappa} \frac{I_1(L_e \kappa)}{I_0(L_e \kappa)} \right]. \tag{14}$$

b. Mixed layer

We can make the stratification more realistic by adding a surface mixed layer:

¹ Over steep topography the barotropic mode is replaced by a bottom-intensified topographic wave mode, which generally cannot be deduced from surface information alone.

$$N = \begin{cases} N_m & \text{if } z > -D \\ N_D e^{(z+D)/h} & \text{if } z \leq -D \end{cases}$$

The mixed layer lies above $z = -D$, and generally $N_m \ll N_D$. The stratification N is thus discontinuous at $z = -D$.

The solution in this case is more involved and is left for the [appendix](#). It consists of a constant stratification solution in the mixed layer and an exponential solution below $z = -D$, which are then matched at $z = -D$. The streamfunction is matched, so that the horizontal velocities are continuous. We also match $(\partial\psi/\partial z)/N^2$, which guarantees continuity of the vertical velocity. This follows from the quasigeostrophic density equation:

$$w = -\frac{f_0}{N^2} \frac{d}{dt} \frac{\partial\psi}{\partial z}. \quad (15)$$

Doing this also makes the PV continuous at $z = -D$.

It will be seen, however, that this condition yields unrealistic solutions, particularly when the mixed layer stratification is weak, so we tested matching the buoyancy instead at the mixed layer base (as would be done in the absence of a discontinuity in N). This produced more realistic density variations both near and below the mixed layer base.

3. Results

We evaluate the analytical solutions using fields from the same North Atlantic simulation discussed by [W13](#). Full model details are given therein. The three regions lie in the western and eastern Atlantic, and in the subpolar gyre ([Fig. 1](#)). In each region we average the density laterally to obtain a profile for $N(z)$ and use the result to fit the analytical N curves. We also calculate the rms density and vorticity as functions of depth, for comparison with the solutions.

The three stratification profiles, with the two idealized fits, are plotted in the left column of [Fig. 2](#). The exponentials were obtained by fitting the deeper portion of N , below the region of rapid variation in the upper several hundred meters. For the mixed layer solution, the stratification N_m was obtained for the shallowest, weakly stratified layer, while the depth D was determined from the position of the maximum of N (about 50 m in regions 1 and 2 and 400 m in region 3). All parameters are listed in [Table 1](#). The values of the deformation radius R_1 range from 22.6 km (region 3) to 32 km (region 2).

The results in [Fig. 2](#) correspond to the *second* mixed layer solution in the [appendix](#), in which $\partial\psi/\partial z$ is matched at $z = -D$. This requires solving a transcendental

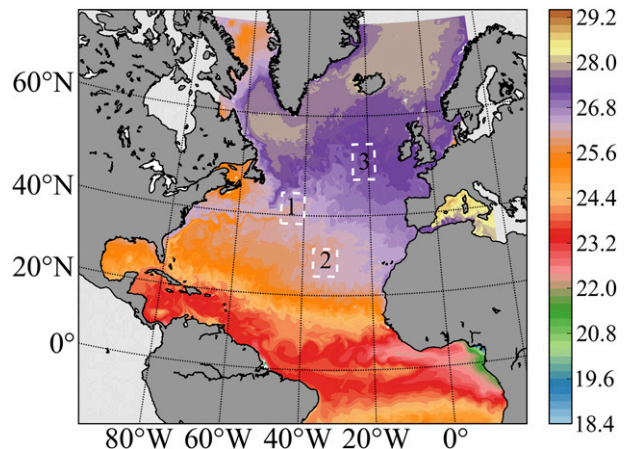


FIG. 1. Surface density from the North Atlantic in the Parallel Ocean Program (POP) simulation of [W13](#). The three regions to be considered are indicated by the stippled boxes (from [W13](#)).

equation, given in [\(A12\)](#). However, the first root varies little for reasonable values of the mixed layer stratification and depth, as indicated in [Table 1](#). Thus, R_1 is well approximated by the pure exponential result [[\(12\)](#)], with the deep stratification N_D replacing the surface value N_0 . As such, neither analytical profile requires a numerical solution for the baroclinic mode.

Shown in the other columns of [Fig. 2](#) are the standard deviations of the density and vorticity plotted against depth. The results for the exponential and mixed layer solutions are shown, as are the curves obtained by [W13](#). The latter derive from a numerical solution for the baroclinic modes, using the actual stratification shown in the left panels.

In region 1, the vorticity deviations ([Fig. 2c](#)) are of similar magnitude for all three solutions, down to roughly 700 m. The density deviations ([Fig. 2b](#)) are also similar, and the solutions capture the subsurface maximum seen near 250-m depth. The exponential and mixed layer solutions behave much the same, though the latter is better in the mixed layer itself; below that, the two yield very similar results. Moreover, both analytical solutions are as successful as the numerical solution of [W13](#).

Similar comments apply in region 2 ([Figs. 2d–f](#)). The vorticity variations are somewhat better for the simple exponential solution, although the differences from the other solutions are small. Interestingly, the two analytical solutions perform better than the full numerical solution in terms of density, as the latter yields much greater variations with depth. Evidently, the analytical fit smooths out the small-scale structures in N , which have little impact on the density variations. Again, the mixed layer solution is most successful in the mixed layer itself.

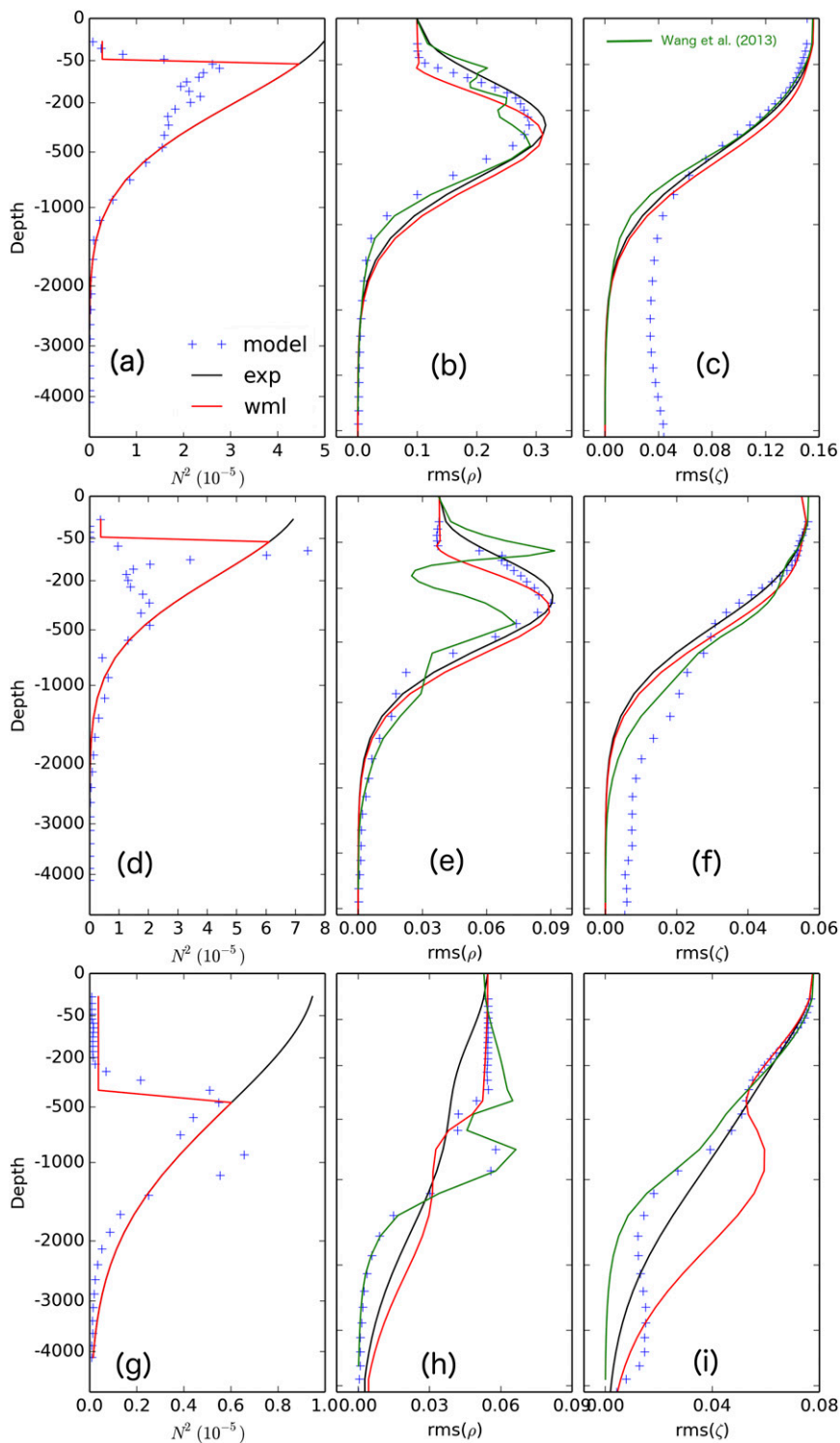


FIG. 2. The horizontally averaged fields from the three regions shown in Fig. 1: (a)–(c) region 1, (d)–(f) region 2, and (g)–(i) region 3. Shown are (left) N^2 , (middle) the rms density anomaly, and (right) the rms vorticity anomaly. The exponential and mixed layer solutions are shown in black and red contours, respectively, and the results from W13 are shown in green. The model fields are indicated by blue plus symbols.

TABLE 1. Parameters for the two N^2 fits. The depth range for the fitting is [380, bottom]. EXP and WML represent the cases with a pure exponential and with a mixed layer overlying an exponential, respectively. The deformation radii come from (12) (EXP) and (A12) (WML). The second estimate for WML (in parentheses) stems from using the exponential estimate [(12)], with N_m replacing N_0 .

Case	1		2		3	
	EXP	WML	EXP	WML	EXP	WML
N_0 (s^{-1})	0.0072	—	0.0085	—	0.0031	—
N_D (s^{-1})	—	0.0068	—	0.0078	—	0.0026
N_m (s^{-1})	—	0.0019	—	0.001	—	0.0005
h (m)	770	770	690	690	2000	2000
MLD (m)	—	50	—	60	—	400
f_0	9.68×10^{-5}	9.68×10^{-5}	7.62×10^{-5}	7.62×10^{-5}	1.14×10^{-4}	1.14×10^{-4}
R_1 (km)	23.8	20.7 (20.8)	32.0	26.7 (26.7)	22.6	15.1 (15.3)

Region 3 differs because the mixed layer is substantially deeper, extending to roughly 400 m. The mixed layer solution accordingly performs better. The predicted density variations are nearly depth independent in the mixed layer itself, as in the model. The exponential solution instead yields density variations that decay monotonically with depth. The full numerical solution varies even more with depth, but in this case the variations are realistic. It performs best below 1000 m, where the analytical solutions are less accurate. However, the differences for the vorticity deviations are much less. All three solutions yield reasonable estimates in the upper 500 m.

Thus, the analytical solutions are generally as good as the reconstructions of W13, despite their idealizations. Including the surface mixed layer improves the density variations in the mixed layer itself but has relatively little impact on the horizontal velocities. Below the mixed layer the simpler exponential fit yields equally good fits for both density and vorticity.

As noted, the mixed layer solution uses an improper matching condition on $\partial\psi/\partial z$ at the base of the mixed layer. The result is that the density is continuous at $z = -D$ but the vertical velocity is not. Matching w instead yields the solution in (A6). The two mixed layer solutions are compared in Fig. 3, using the region 3 fields.

Matching $(\partial\psi/\partial z)/N^2$ instead of $\partial\psi/\partial z$ produces a discontinuity in the density variations at the mixed layer base. The variations in the mixed layer in the former solution are smaller than in the latter, and they are much larger below. The vorticity deviations in the mixed layer are also better captured by the solution with a continuous density; the other solution grossly overestimates the variations. But while both solutions produce too large deviations below the mixed layer, the continuous w solutions are much greater, producing the appearance of a discontinuity at the mixed layer base. The curve is actually continuous, but the deviations increase greatly over a small depth range.

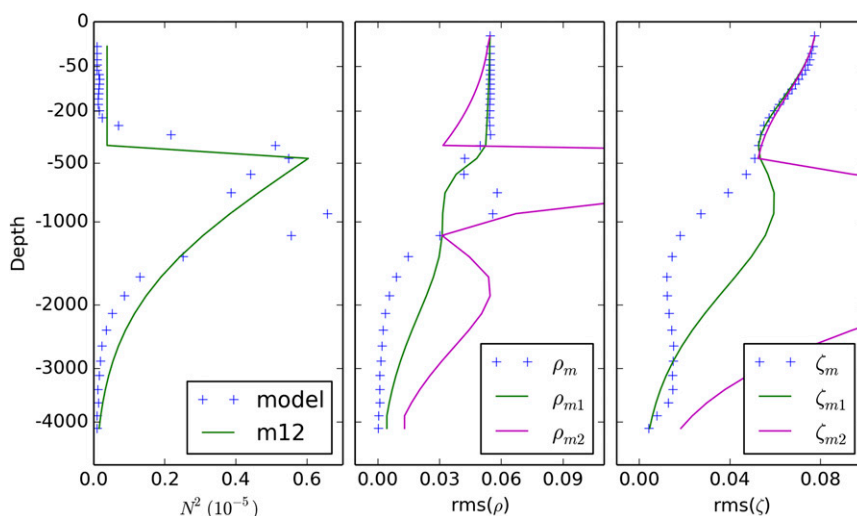


FIG. 3. Comparing the two mixed layer solutions, the solution in which $\partial\psi/\partial z$ is matched at the mixed layer base (in green) and that in which $(\partial\psi/\partial z)/N^2$ is matched instead (in purple). The fields are from region 3, and the panels shown (left) N^2 , (middle) rms density, and (right) rms vorticity.

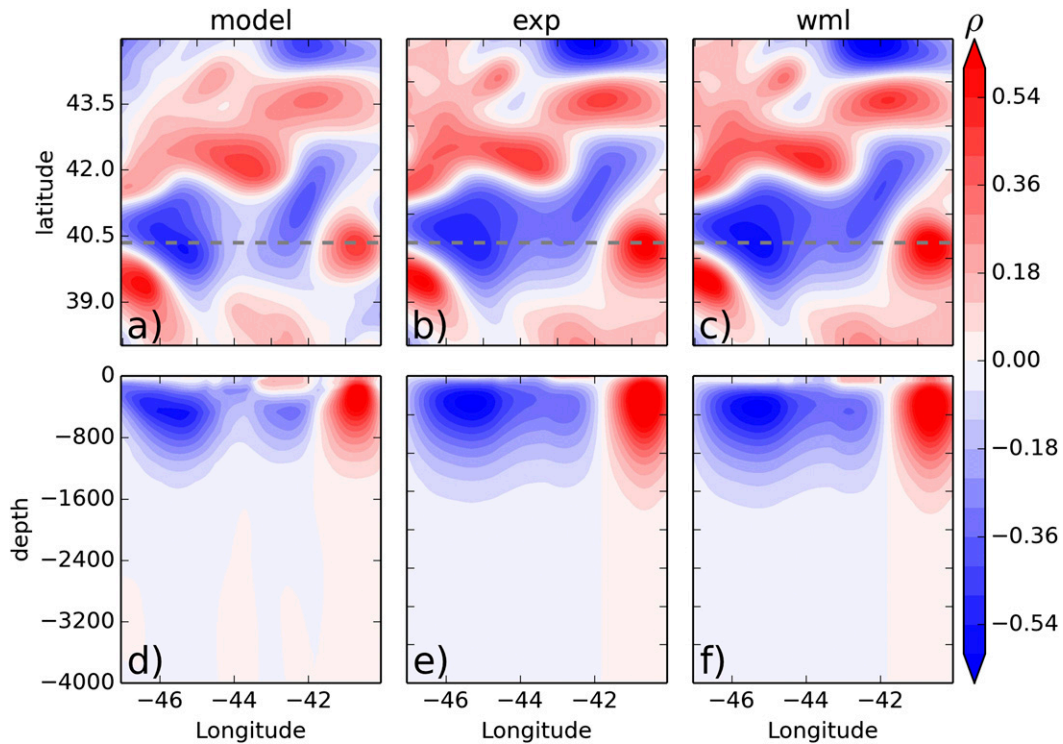


FIG. 4. Plan views from region 1 of the density anomaly at 520-m depth for (a) the model, (b) the pure exponential fit, and (c) the exponential with the mixed layer. (d)–(f) Vertical slices of the density anomaly along the dashed line indicated in the upper panels.

A third solution was also tested, in which N was assumed to increase exponentially to the base of the mixed layer and decay exponentially below (see the appendix). While the results (not shown) were better than with the continuous w solution above, they were still significantly worse than with the continuous density solution.

Thus, we retain the mixed layer solution that matches $\partial\psi/\partial z$ at $z = -D$. This is obviously a practical choice rather than a rigorous one, as the solution implies discontinuous vertical velocities. The unrealistic element is the discontinuity in N , as the model profiles are instead continuous. We retain the continuous density solution in the interest of having a relatively simple analytical profile.

Further comparisons are shown in the subsequent figures. Snapshots of the density anomaly in region 1 are shown in Fig. 4. The model fields are in the left column and the exponential and mixed layer solutions are in the middle and right columns, respectively. Figures 4a–c show plan views of the density anomalies at 520-m depth, and Figs. 4d–f show density cross sections taken along the dashed line in the upper panels, near 40.5°N.

Both analytical solutions capture the horizontal structure and amplitude of the model anomalies (Figs. 4a–c), beyond relatively minor regional differences. Note that 520 m is well below the mixed layer depth (roughly 50 m).

The vertical structure (Figs. 4d–f) is also very similar. The analytical solutions decay more slowly with depth, a consequence of using only a single baroclinic mode in the decomposition. Nevertheless, the overall picture is very similar. The mixed layer solution is slightly better in the mixed layer itself, capturing, for example, the vertical variations near 43°W, but the exponential solution is basically as good.

The comparisons in region 2 are very similar and are not shown. The fields for region 3 are contoured in Fig. 5. The depth (520 m) for the plan views is just below the mixed layer (400 m). Again, the structures and amplitudes are very similar, outside of regional variations. Differences are more apparent in the vertical though, with the mixed layer solution clearly superior at capturing the variations in and just below the mixed layer. Again, the decay below the mixed layer is too gradual in both solutions because of having only a single baroclinic mode.

The vorticity fields compare similarly. In region 1 (Fig. 6), the two solutions produce realistic structures with reasonable amplitudes. The vertical slices too are very similar, above 800 m. However, the model anomalies extend deeper than in the solutions, which is unsurprising given that the barotropic component is absent in the solutions. But the result is good in the upper part

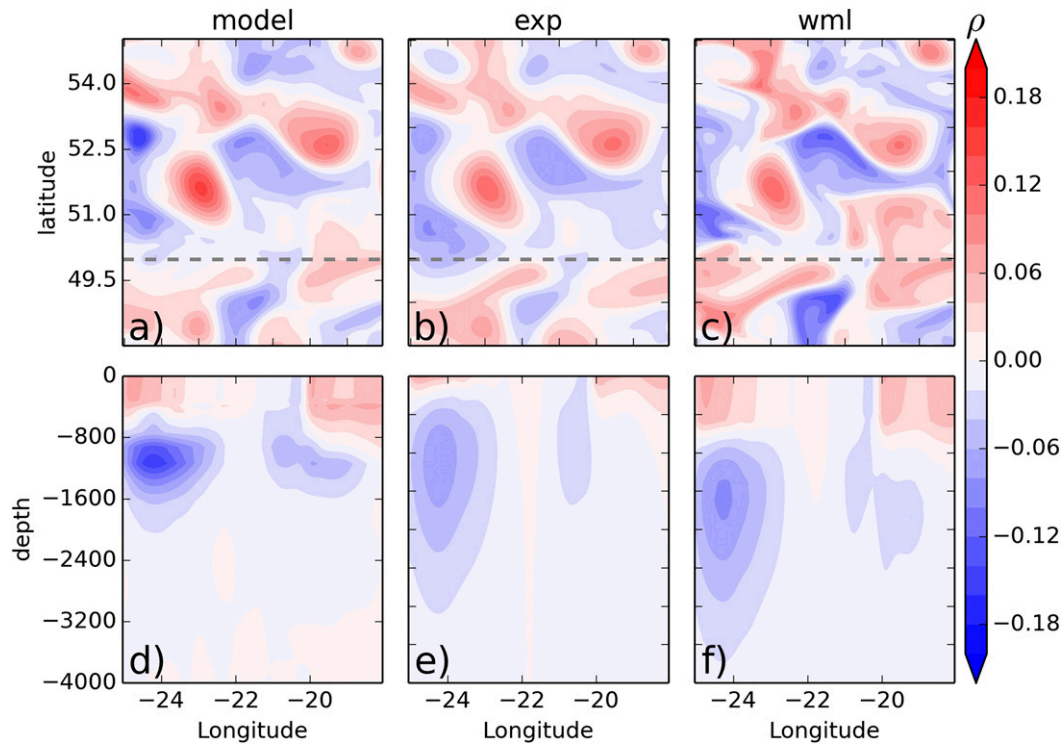


FIG. 5. As in Fig. 4, but for region 3.

of the water column, and there is no appreciable improvement with the mixed layer model.

Similar comments apply in region 3 (Fig. 7). The solutions are comparable in the upper 1000 m, but the model vorticity anomalies extend deeper. And here too, the mixed layer yields only minor changes from the pure exponential.

The similarities between the solutions and the model are quantified in Fig. 8, which shows the correlations between the analytical solutions and the model density (left) and vorticity (right) as functions of depth. In region 1 (top panels), the correlations for the density for both solutions (solid contours) are between 0.8 and 1.0 in the upper 1000 m. The correlations for the vorticity are similarly high. Moreover, the two solutions are not greatly different.

W13 found that the SQG contribution to the full solution was generally less than that of the baroclinic modes. We examined this by calculating the correlations for the SQG portions alone (dashed contours in Fig. 8). The correlations for the density are comparable to those for the full solutions in the upper 50 m. This is as expected, since the SQG solution matches the model density at the surface, but the correlations decrease below the mixed layer; at 500 m they are nearer to 0.5 for both analytical profiles. Of course, the correlations do not reflect the amplitude of the SQG contribution, and

the latter decrease even more rapidly in comparison to the model's (not shown). The correlations for the SQG vorticity (right panel) are lower even at the surface, being slightly less than 0.6. This reflects that the surface density is not always aligned with the surface pressure (W13). Thus, the baroclinic mode contribution is more important in this regard.

The results are qualitatively the same in the other two regions (middle and bottom panels). It is striking in particular that the two idealized profiles yield such similar correlations. Despite that the mixed layer improves the amplitude of the density variations in the mixed layer, it changes the structures little.

4. Summary and conclusions

We extended the study of W13 for predicting subsurface velocities and density from surface buoyancy and sea surface height. We use analytical solutions to make the vertical projection, assuming either an exponential N profile or an exponential with a mixed layer at the surface. The solution is a combination of an SQG component and the first baroclinic mode.

The solutions perform remarkably well in comparison with subsurface fields from a North Atlantic simulation. Both the density and vorticity fields are realistic, above about 1000 m depth. Moreover, the comparisons are

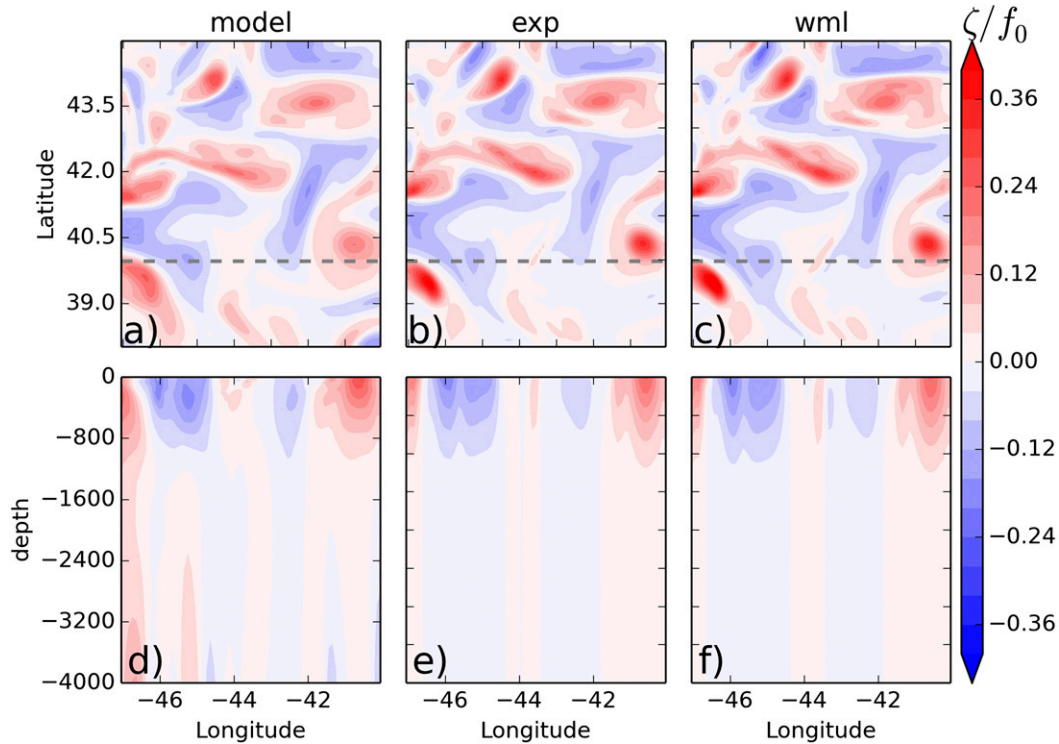


FIG. 6. Plan views of the vorticity (normalized by f_0) and vertical slices of the same quantity at 520-m depth in region 1.

generally as good as those of W13, who used numerical solutions to obtain the vertical dependence.

Several additional points are of interest. Including a surface mixed layer improves the density fields in the mixed layer itself but has little effect below. Also, both solutions yield similar vorticity fields. This suggests that a simple exponential profile may suffice in many applications, and this can be easily determined from climatological density.

Second, the reconstructions require only a single baroclinic mode. We have dispensed with the barotropic mode and accordingly miss variability at great depths, but this is to be expected as the fields are reconstructed solely from surface data. Nevertheless, if a barotropic mode is desired, a flat bottom condition can be applied, as with the exponential N solution of LaCasce (2012). Then the two unknown modal amplitudes would be determined as in W13. The price would be having to solve a transcendental equation for the baroclinic modes, something we have avoided here.

The mixed layer solution has a discontinuity at the base of the mixed layer, and the solutions require matching conditions there. Matching the density rather than the vertical velocity yields better results, despite that the latter is theoretically preferable. The reasoning is that the weakly stratified mixed layer is always joined

to the stratified interior via a transition region, so that the density is continuous. Including such a layer in the theoretical model is possible but would defeat the purpose of having a simplified solution.

We found too that the SQG portion of the solution is most important in the mixed layer, where the stratification is weak and the PV near zero. Thus, the SQG construction is probably most valuable as an idealized representation of mixed layer flow.

Acknowledgments. It is with pleasure and sadness that we acknowledge Bach Lien Hua, a good friend and an inspiration. She made major contributions to oceanography, in problems like the one considered here. Thanks to two anonymous reviewers, Paola Cessi, Bill Young, and Jörn Callies for diverse comments. The work was supported in part by NSF Grant OCE-1234473 (Wang) and by the Norwegian Research Council Grant 221780, NORSEE (LaCasce).

APPENDIX

The Mixed Layer Solutions

The stratification is

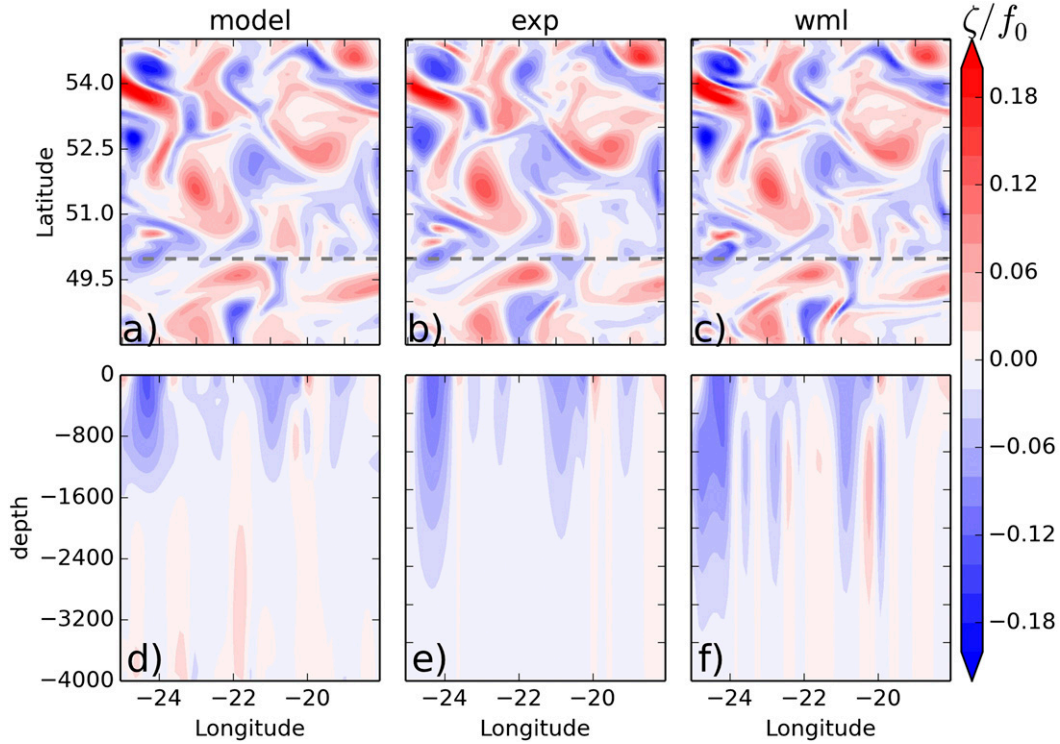


FIG. 7. As in Fig. 6, but for region 3.

$$N = \begin{cases} N_m & \text{if } z > -D \\ N_D e^{(z+D)/h} & \text{if } z \leq -D \end{cases}$$

$$\Delta = N_m \kappa \left[\frac{N_m}{N_D} \cosh(L_m \kappa) I_0(L_D \kappa) + \sinh(L_m \kappa) I_1(L_D \kappa) \right], \tag{A5}$$

The SQG solution in the mixed layer that satisfies the upper boundary condition is

$$\hat{\psi} = A_1 \cosh\left(\frac{N_m \kappa z}{f_0}\right) + \frac{\hat{b}}{N_m \kappa} \sinh\left(\frac{N_m \kappa z}{f_0}\right). \tag{A1}$$

The solution in the lower region, which vanishes with depth, follows from (8):

$$\hat{\psi} = A_2 e^{(z+D)/h} I_1[L_D \kappa e^{(z+D)/h}], \tag{A2}$$

with $L_D \equiv N_D h / f_0$. We obtain A_1 and A_2 by matching $\hat{\psi}$ and $(\partial \hat{\psi} / \partial z) / N^2$ at $z = -D$. As noted, this guarantees continuity of the horizontal and vertical velocities, respectively. The result is

$$A_1 = \frac{\hat{b}}{\Delta} \left[\frac{N_m}{N_D} \sinh(L_m \kappa) I_0(L_D \kappa) + \cosh(L_m \kappa) I_1(L_D \kappa) \right], \tag{A3}$$

$$A_2 = \frac{\hat{b}}{\Delta}, \text{ and} \tag{A4}$$

with $L_m \equiv N_m D / f_0$. In the limit of vanishing surface stratification, ψ is nearly barotropic in the mixed layer and proportional to the surface buoyancy.

The derivation for the baroclinic modes is similar. The upper and lower solutions that satisfy the boundary conditions are

$$\hat{\psi} = \begin{cases} B_1 \cos\left(\frac{L_m z}{R_n D}\right) & \text{if } z > -D \\ B_2 e^{(z+D)/h} J_1\left[\frac{L_D}{R_n} e^{(z+D)/h}\right] & \text{if } z \leq -D \end{cases}$$

Matching $\hat{\psi}$ and $(\partial \hat{\psi} / \partial z) / N^2$ at $z = -D$ yields a transcendental equation for the R_n :

$$\frac{N_m}{N_D} J_0\left(\frac{L_D}{R_n}\right) - \tan\left(\frac{L_m}{R_n}\right) J_1\left(\frac{L_D}{R_n}\right) = 0. \tag{A6}$$

We solve (A6) numerically, using Newton's method.

Thus, the total streamfunction in the mixed layer case is

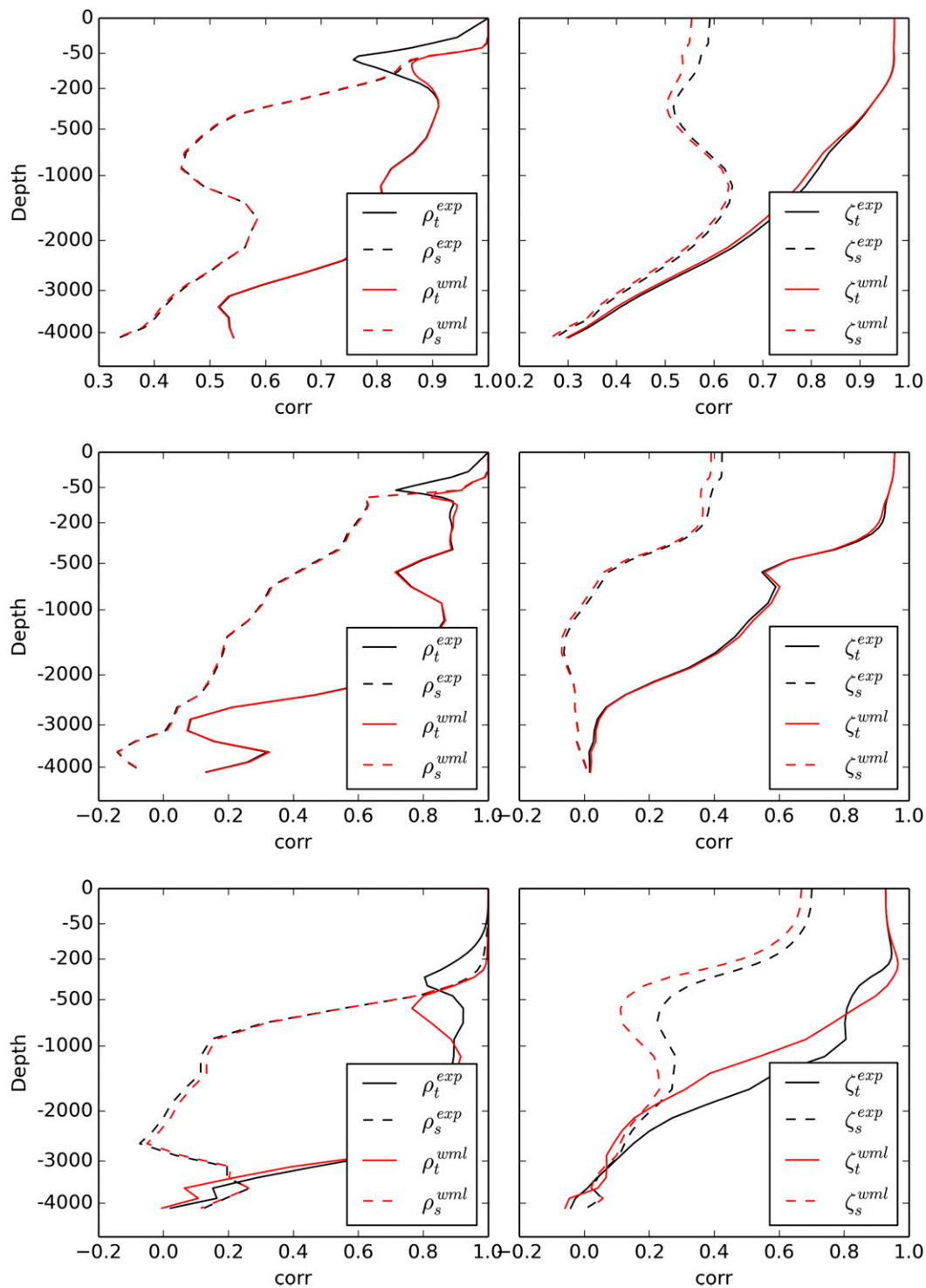


FIG. 8. Correlations between the predicted and modeled (left) density and (right) vorticity for (a) region 1, (b) region 2, and (c) region 3. Shown are the results using the single exponential (black solid curves) and mixed layer (red solid curves) solutions, as well as the correlations from the SQG portions alone (dashed curves).

$$\psi = \begin{cases} A_1 \cosh\left(\frac{L_m \kappa z}{D}\right) + \frac{\hat{b}}{N_m \kappa} \sinh\left(\frac{L_m \kappa z}{D}\right) + \gamma_1 \cos\left(\frac{L_m z}{R_n D}\right) & z > -D \\ A_2 e^{(z+D)/h} I_1[L_D \kappa e^{(z+D)/h}] + \gamma_1 e^{(z+D)/h} \cos\left(\frac{L_m}{R_n}\right) \frac{J_1[L_D e^{(z+D)/h}/R_n]}{J_1(L_D/R_n)} & z \leq -D \end{cases}. \quad (\text{A7})$$

The constant γ_1 is determined again from the surface elevation. As this only involves the mixed layer solution, the result is particularly simple:

$$\gamma_1 = \frac{g}{f_0} \hat{\eta} - A_1. \quad (\text{A8})$$

The solution obtained by matching $\partial\psi/\partial z$ instead at $z = -D$ is very similar. Having a continuous buoyancy at the interface with a discontinuous N is equivalent to having a delta-function PV sheet at the mixed layer base. Such a discontinuity can support buoyancy anomalies (Bretherton 1966; Plougonven and Vanneste 2010; Smith and Bernard 2013), which in turn can permit Eady-type instabilities in the mixed layer (Pedlosky 1987). For the present solutions, however, the density anomaly is assumed confined to the upper surface, precluding instability.

The constants for the SQG solution are instead

$$A_1 = \frac{\hat{b}}{\Delta} \left[\frac{N_D}{N_m} \sinh(L_m \kappa) I_0(L_D \kappa) + \cosh(L_m \kappa) I_1(L_D \kappa) \right], \quad (\text{A9})$$

$$\hat{\psi} = \begin{cases} A_1 \cosh(L_m \kappa) + \frac{\hat{b}}{N_m \kappa} \sinh\left(\frac{L_m \kappa z}{D}\right) + \gamma_1 \cos\left(\frac{2.4048 L_m z}{L_D D}\right) & z > -D \\ A_2 e^{(z+D)/h} I_1[L_D \kappa e^{(z+D)/h}] + \gamma_1 e^{(z+D)/h} \cos\left(\frac{2.4048 L_m}{L_D}\right) \frac{J_1[2.4048 e^{(z+D)/h}]}{J_1(2.4048)} & z \leq -D \end{cases}.$$

The constant γ_1 is again determined by (A8).

A third solution was also tested, involving a double exponential stratification profile:

$$N = \begin{cases} N_D e^{-(z+D)/h_m} & \text{if } z > -D \\ N_D e^{(z+D)/h} & \text{if } z \leq -D \end{cases}.$$

In fact, this provides the most satisfactory fit to the density profiles in the three cases considered, and the stratification is continuous, so that density alone can be matched at $z = -D$. But the results were as unsatisfactory, as with the first solution described above. The density variations increased below the surface to unrealistically large values near the mixed layer base, and the vorticity variations were overly large at depth, so we chose to focus on the second solution given above.

$$A_2 = \frac{\hat{b}}{\Delta}, \quad \text{and} \quad (\text{A10})$$

$$\Delta = N_D \kappa \cosh(L_m \kappa) I_0(L_D \kappa) + N_m \kappa \sinh(L_m \kappa) I_1(L_D \kappa). \quad (\text{A11})$$

The transcendental equation for the baroclinic modes is also altered slightly, to

$$J_0\left(\frac{L_D}{R_n}\right) + \frac{N_m}{N_D} \tan\left(\frac{L_m}{R_n}\right) J_1\left(\frac{L_D}{R_n}\right) = 0. \quad (\text{A12})$$

The form is slightly different than before, and in the limit of weak surface stratification the second term is very small. So, in fact, the solutions are close to the zeros of J_0 . As such, one can approximate R_1 by $L_D/2.4048$ in the full solution.

Thus, the total streamfunction can be written as before, but with the approximate value of R_1 :

REFERENCES

- Blumen, W., 1978: Uniform potential vorticity flow. Part I: Theory of wave interactions and two-dimensional turbulence. *J. Atmos. Sci.*, **35**, 774–783, doi:10.1175/1520-0469(1978)035<0774:UPVFPI>2.0.CO;2.
- Bretherton, F. P., 1966: Critical layer instability in baroclinic flows. *Quart. J. Roy. Meteor. Soc.*, **92**, 325–334, doi:10.1002/qj.49709239302.
- Held, I., R. Pierrehumbert, S. Garner, and K. Swanson, 1995: Surface quasi-geostrophic dynamics. *J. Fluid Mech.*, **282**, 1–20, doi:10.1017/S0022112095000012.
- Isern-Fontanet, J., B. Chapron, G. Lapeyre, and P. Klein, 2008: Potential use of microwave sea surface temperatures for the estimation of ocean currents. *Geophys. Res. Lett.*, **33**, L24608, doi:10.1029/2006GL027801.
- LaCasce, J., 2012: Surface quasigeostrophic solutions and baroclinic modes with exponential stratification. *J. Phys. Oceanogr.*, **42**, 569–580, doi:10.1175/JPO-D-11-0111.1.

- , and A. Mahadevan, 2006: Estimating subsurface horizontal and vertical velocities from sea surface temperature. *J. Mar. Res.*, **64**, 695–721, doi:[10.1357/002224006779367267](https://doi.org/10.1357/002224006779367267).
- Lapeyre, G., 2009: What vertical mode does the altimeter reflect? On the decomposition in baroclinic modes on a surface-trapped mode. *J. Phys. Oceanogr.*, **39**, 2857–2874, doi:[10.1175/2009JPO3968.1](https://doi.org/10.1175/2009JPO3968.1).
- , and P. Klein, 2006: Dynamics of the upper oceanic layers in terms of surface quasigeostrophy theory. *J. Phys. Oceanogr.*, **36**, 165–176, doi:[10.1175/JPO2840.1](https://doi.org/10.1175/JPO2840.1).
- Pedlosky, J., 1987: *Geophysical Fluid Dynamics*. 2nd ed. Springer-Verlag, 728 pp.
- Plougonven, R., and J. Vanneste, 2010: Quasigeostrophic dynamics of a finite-thickness tropopause. *J. Atmos. Sci.*, **67**, 3149–3163, doi:[10.1175/2010JAS3502.1](https://doi.org/10.1175/2010JAS3502.1).
- Samelson, R. M., 1992: Surface-intensified Rossby waves over rough topography. *J. Mar. Res.*, **50**, 367–384, doi:[10.1357/002224092784797593](https://doi.org/10.1357/002224092784797593).
- Smith, K. S., and E. Bernard, 2013: Geostrophic turbulence near rapid changes in stratification. *Phys. Fluids*, **25**, 046601, doi:[10.1063/1.4799470](https://doi.org/10.1063/1.4799470).
- Tulloch, R., and K. S. Smith, 2006: A theory for the atmospheric energy spectrum: depth-limited temperature anomalies at the tropopause. *Proc. Natl. Acad. Sci. USA*, **51**, 2756–2768.
- Wang, J., G. R. Flierl, J. H. LaCasce, J. L. McClean, and A. Mahadevan, 2013: Reconstructing the Ocean's Interior from Surface Data. *J. Phys. Oceanogr.*, **43**, 16111626.